



Simulation of rainfall–runoff processes in karst catchment considering the impact of karst depression based on the tank model

Xianmeng Meng¹ · Meng Huang¹ · Dengfeng Liu² · Maosheng Yin¹

Received: 15 July 2020 / Accepted: 8 January 2021 / Published online: 5 February 2021
© Saudi Society for Geosciences 2021

Abstract

Karst depressions play an important role in runoff generation and concentration processes of karst catchments. Storm water tends to be stored in karst depressions firstly before routing to the catchment outlet. However, simulating methods of runoff processes considering the impact of karst depressions are rarely reported. To fill this concept and technology gap, we propose a conceptual hydrological model considering the role of karst depressions in this study. A three serial tank model coupled with two soil tanks is established at each grid in each subcatchment, to simulate surface runoff, interflow, groundwater runoff, and soil moisture dynamics. During the process of flow concentration, surface runoff from each grid is reduced by karst depressions at its lower reach. The surface runoff loss is controlled by the area ratio of karst depression and corresponding subcatchment. River channel routing is carried out based on the Muskingum approach. The conceptual hydrological model is further calibrated and validated over the Hamajing catchment, a small karst catchment in Hubei Province, China. Results show that the proposed model can generally reproduce the runoff generation and concentration processes well. Nash-Sutcliffe efficiency (NSE) coefficient is 0.85 during the calibration period and 0.78 in the validation period. Root mean squared errors are 6.24 m³/s and 5.35 m³/s during calibration and validation periods respectively. Sensitivity analysis indicates that the parameters related to the first tank are most sensitive to the simulation results, whereas the change of parameters related to the second and third tanks cannot significantly influence the simulation results. Additionally, the area ratio of karst depression has great influence on the runoff processes in karst catchment. This proposed conceptual model provides a simple approach to simulate the hydrological processes in karst region.

Keywords Hydrological processes · Karst catchment · Karst depression · Tank model

Introduction

On the earth, karst terrains cover about 15% of the total land, and their landscape is characterized by the dissolving action of water on carbonate bedrock (usually limestone, dolomite, or marble). Besides, over 1 billion people (17% of the world's population) live and rely on karst water to survive (Li et al. 2006). In China, Yunnan-Guizhou Plateau is a typical region with large and continuous karst area owning carbonate rocks

of about 7.8×10^5 km² and exposed carbonate rocks of more than 5.0×10^5 km². Compared with the other region, karst catchment is more vulnerable to drought because of natural and artificial factors. The particular feature of carbonate rocks makes the soils in the karst region very thin (30–50 cm in thickness) (Zhang et al. 2011), which cannot hold enough water. Artificial factors, such as deforestation and agriculture, accelerate soil erosion and loss of water and cause ecological environment deterioration. From September 2009 to May 2010, southwest of China was attacked by a rare severe autumn-winter-spring drought, leading to more than 20 million people lacking necessary drinking water. In order to reasonably exploit water resources and protect ecological environment, it is very urgent to do research on the rules of hydrological cycle in karst region.

Because of calcareous formations, a lot of fissured and cavernous geomorphology with sinkholes and cavities exist in karst region (Mangin 1975). This complex structure causes different hydraulic conditions from those in a general

Responsible Editor: Amjad Kallel

✉ Xianmeng Meng
mengxianmeng2000@163.com

¹ School of Environmental Studies, China University of Geosciences, Wuhan 430074, China

² School of Water Resources and Hydropower, Xi'an University of Technology, Xi'an 710048, China

catchment. When the precipitation occurs, the hydrological processes are very complicated, so different types of water flow such as crack and pipeline flow may coexist in karst region. And we have to describe them with different equations. Meanwhile, surface water and groundwater can change to each other frequently. As the structure of karst aquifer system is very complicated, it is difficult to develop a karstic hydrological model. First of all, the detailed structure of karst aquifer system containing sinkholes, cavities, and conduits network is unknown to us. Thus, it is impossible to have a good understanding of the hydrological processes in karst region. Secondly, even if we can obtain the detailed structure of karst aquifer system by advanced equipment, the application of model to karst region is still difficult. It is because karst catchments, generally located in the remote and mountainous areas of China, have not enough observed data to calibrate and verify the established model. Therefore, how to utilize the existing data to establish a simple hydrological model is an effective approach to analyze the hydrological cycle in karst region.

Karst hydrological model can be divided into systematic simulation model and physical process-based simulation model. Systematic simulation model often employs empirical or pure mathematical equations to establish a relationship between input and output hydrological time series (Hao et al. 2006). A variety of mathematical methods, including kernel function (Dreiss 1982, 1983; Labat et al. 2000a; Jukic and Denic-Jukic 2006), artificial neural networks (Lambrakis et al. 2000; Hu et al. 2008; Meng et al. 2015), wavelet analysis (Labat et al. 2000b; Labat et al. 2001), and regression analysis (Felton and Currens 1994), has been successfully applied to simulate the hydrological processes in the karst region. Recently, Fan et al. (2013) proposed an assembled extreme value statistical model to obtain the extreme distribution of karst spring discharge depletion.

With the gradual deepening of understanding in karst hydrological processes and the development of computer, the process-based mechanism model has appeared. According to whether or not the mass and momentum conservation equations are involved, process-based mechanism model can be further classified into conceptual model and physically based model (Hu and Tian 2007). The conceptual model uses simplified physical interpretation such as series of linear or non-linear reservoirs to describe the process from precipitation to hydrograph (Barrett and Charbeneau 1997; Halihan and Wicks 1998; Padilla and Pulido-Bosch 2008). The physically based model uses partial differential equations of the mass and momentum conservation to simulate hydrological processes (Freeze and Harlan 1969). The effect of conduit and fracture network has been added to finite differential model (Sun et al. 2005) and finite element model (Eisenlohr et al. 1997) to simulate karst hydrological processes. Distributed hydrological models such as SWMM (Campbell and Sullivan 2002), modified WetSpa (Liu et al. 2005), modified SWAT

(Palanisamy and Workman 2015; Amin et al. 2017), and coupled Liuxihe model with PERSIANN-CCS QPEs (Li et al. 2019) are occupied to analyze the characteristics of karst hydrological processes in different conditions.

Although most of previous studies can well reproduce the hydrological processes, they have some limitations. In the karst region, many depressions are created under the process of karstification, which have significant effect on the processes of runoff generation and concentration. During the storm period, much water stored in karst depressions could not be routed to the catchment outlet cross section leading to the discharge smaller than that of the general catchment. The impact of karst depressions is not involved in previous models. This neglect in previous models may be due to the difficulty in quantitatively simulating runoff process in karst catchment. However, neglect of the impact of karst depressions in simulating runoff process within karst catchment may lead to misinterpretations of actual observations and measurements. Therefore, appropriate modification is needed for previous rainfall-runoff model during the application in karst catchment. To the best of our knowledge, the impact of karst depression on rainfall-runoff modeling has not been addressed systematically in literature.

In this paper, we propose a conceptual hydrological model considering the role of karst depressions. Based on digital elevation model, the depression areas are extracted. A three-tank model coupled with two soil tanks is established at each grid in each subcatchment, to simulate surface runoff, interflow, groundwater runoff, and soil moisture dynamics. During the process of flow concentration, surface runoff from each grid is reduced by karst depressions at its lower reach. The runoff loss is calculated based on the area ratio of karst depression divided by the depression extracted by DEM. River channel routing is carried out based on the Muskingum approach. This model is applied at a small karst catchment in Hubei province, China. After the model is calibrated and validated, it is used to quantify the effect of karst depression. The aim of this paper is to shed more light on the phenomena how the flood is stored in karst depressions. Perhaps it will encourage public and scientific concern that should lead to a more complete mathematical or physical model to describe the specificity of hydrological processes in the karst region. The rest of the paper is organized as follows: the development and detailed description of the model proposed in this study are presented in the section “Model description and development.” The “Study area” section introduces information on the study area including the geographic location, hydrological condition, and topography information. Model calibration and verification as well as simulation results are presented in the “Results” and “Discussion” sections. In the “Summary and conclusions” section, the main conclusions and future work are presented.

Model description and development

Outline of hydrological model

The proposed hydrological model is based on the standard tank model (Sugawara 1972), which belongs to a deterministic, lumped, and conceptual model, using a series of vertically laid tanks to simulate the runoff generation processes. And bottom outlets and side outlets of these tanks represent infiltration and runoff processes respectively. Because of the simple structure of the tank model, only requiring precipitation, runoff, and evapotranspiration observations to run, it is recommended by the World Meteorological Organization as a hydrological forecasting model (WMO 1981) to simulate either flood events or long-term runoff from catchment. Through the application of tank model in Asia, Africa, Europe, and the USA, good simulated rainfall–runoff processes have been acquired.

In this study, using a global digital elevation model (DEM), subcatchments and river networks are extracted through flow direction analysis, flow accumulation analysis, and catchment recognition under the platform of hydrology package in ARCGIS 10. Each grid at the subcatchment is a combination of a three-serial tank model coupled with two soil tanks (Fig. 1), while a detailed explanation of the symbols is provided in Table 1, and the calculation of runoff and infiltration is explained by Huang et al. (2007). The total discharge includes surface runoff, interflow, and groundwater runoff produced by each grid. The total runoff concentrates into the outlet of subcatchment and then outlet of catchment by river networks. The flowchart of the proposed hydrological model is shown in Fig. 2.

Influence of karst depressions on subcatchment outlet discharge

Using the ARCGIS software, the depressions in the whole catchment could be recognized based on DEM. It is noteworthy that accurate identification of karst depressions is quite difficult (if not impossible) even in a small catchment. The depressions recognized by DEM may contain several types of depressions. Therefore, it is assumed that the karst depressions are composed of some of these depressions recognized by DEM, and the parameter α is used to describe the ratio of karst depression to depression recognized by DEM. The value of α can be determined by empirical estimation and/or parameter calibration. During the process of flow concentration in each subcatchment, surface runoff loss will occur because of the existence of karst depressions. If the surface runoff generated from a grid wants to be routed to the outlet of subcatchment, it has to experience the loss produced by the karst depressions in its lower reach. Hence, the surface runoff from a grid needs to

be deducted by $R'_{is}(t) \frac{\alpha A'_j}{A_j}$, with the rest $R'_{is}(t) \left(1 - \frac{\alpha A'_j}{A_j}\right)$ continuing to the next lower part, and so forth (Fig. 3). It is noteworthy that, for a specific depression, the shape (including depth, slope, and area) may have obvious impact on the capacity of the depression. However, fully detailed survey of depressions in a karst catchment may be toilsome and unnecessary. To overcome this problem, we centralize all these impacts of depressions in the conceptual parameter α . Parameter sensitivity analysis of α as well as other parameters will be conducted later in the present study. The surface runoff that can be routed to the outlet of subcatchment is obtained as follows:

$$R_{is}(t) = R'_{is}(t) \prod_{j=1}^k \left(1 - \frac{\alpha A'_j}{A_j}\right) \tag{1}$$

where $R'_{is}(t)$ is surface runoff yield from a grid; A'_j is the area of one depression recognized by DEM; A_j is the area with the same length as A'_j from the outlet of subcatchment; α is the ratio of karst depression divided by the depression extracted by DEM; k is the total number of depressions in the lower reach of the grid.

In the karst depressions, only evaporation occurs. The total runoff from the whole subcatchment is the sum of runoff from each grid

$$R(t) = \sum_{i=1}^n R_{is}(t) + \sum_{i=1}^m R_{iL}(t) + \sum_{i=1}^m R_{ig}(t) \tag{2}$$

where $R_{iL}(t)$ and $R_{ig}(t)$ are interflow and groundwater runoff yields of each grid respectively; m is the total number of grids; n is the total number of grids except depression.

The total discharge at the outlet of subcatchment is expressed as

$$Q(t) = \frac{A}{\Delta t} R(t) \tag{3}$$

where Δt is a time step, and A is the area of grid.

Flow routing

On the basis of the runoff yield at each grid and runoff loss produced by karst depressions, the discharge of each subcatchment outlet can be obtained. Then, the river channel routing method employs the classical Muskingum routing equation of McCarthy (1938) because of its simplicity (McCarthy 1938). In mathematical equation, inflow I , outflow O , and storage S in Muskingum method are written as

$$S = K[XI + (1-X)O] \tag{4}$$

where K is storage constant (T), and X is relative importance of inflow and outflow to the storage in the reach.

Table 1 Description of symbols used in the hydrological model

Symbol	Description	Quantity dimension
P	Precipitation	LT^{-1}
E_p	Potential evapotranspiration	LT^{-1}
y_{A1}	Lower surface runoff	LT^{-1}
y_{A2}	Upper surface runoff	LT^{-1}
y_{A0}	Infiltration of the first tank	LT^{-1}
y_{B1}	Intermediate runoff	LT^{-1}
y_{B0}	Infiltration of the second tank	LT^{-1}
y_{C1}	Groundwater runoff	LT^{-1}
H_{A1}	Lower runoff threshold of the first tank	L
H_{A2}	Upper runoff threshold of the first tank	L
H_{B1}	Runoff threshold of the second tank	L
H_{C1}	Runoff threshold of the third tank	L
S_1	Saturation capacity of primary soil moisture storage	L
S_2	Saturation capacity of secondary soil moisture storage	L
K_1	Water transfer between the primary and secondary soil storage	LT^{-1}
A_0	Infiltration coefficient of the first tank	T^{-1}
A_1	Coefficient of the lower surface runoff	T^{-1}
A_2	Coefficient of the upper surface runoff	T^{-1}
B_0	Infiltration coefficient of the second tank	T^{-1}
B_1	Coefficient of the intermediate runoff	T^{-1}
C_1	Coefficient of the groundwater runoff	T^{-1}
X_A	Water storage in the first tank	L
X_B	Water storage in the second tank	L
X_C	Water storage in the third tank	L
X_p	Primary soil moisture storage	L
X_s	Secondary soil moisture storage	L

The continuity equation is given by

$$\frac{dS}{dt} = I - O \tag{5}$$

The Muskingum method based on Eq. (4) and (5) can be expressed as

$$O^{n+1} = C_1 I^{n+1} + C_2 I^n + C_3 O^n \tag{6}$$

where

$$C_1 = \frac{0.5\Delta t - XK}{0.5\Delta t + (1-X)} \quad K \quad C_2 = \frac{0.5\Delta t + XK}{0.5\Delta t + (1-X)} \quad K \quad C_3 = -0.5\Delta t + (1-X) \frac{K}{0.5\Delta t + (1-X)} \quad K \tag{7a, b, c}$$

where Δt is a time step, I^n and O^n are inflow and outflow at the beginning of the time step, respectively, and I^{n+1} and O^{n+1} are inflow and outflow at the end of the time step, respectively.

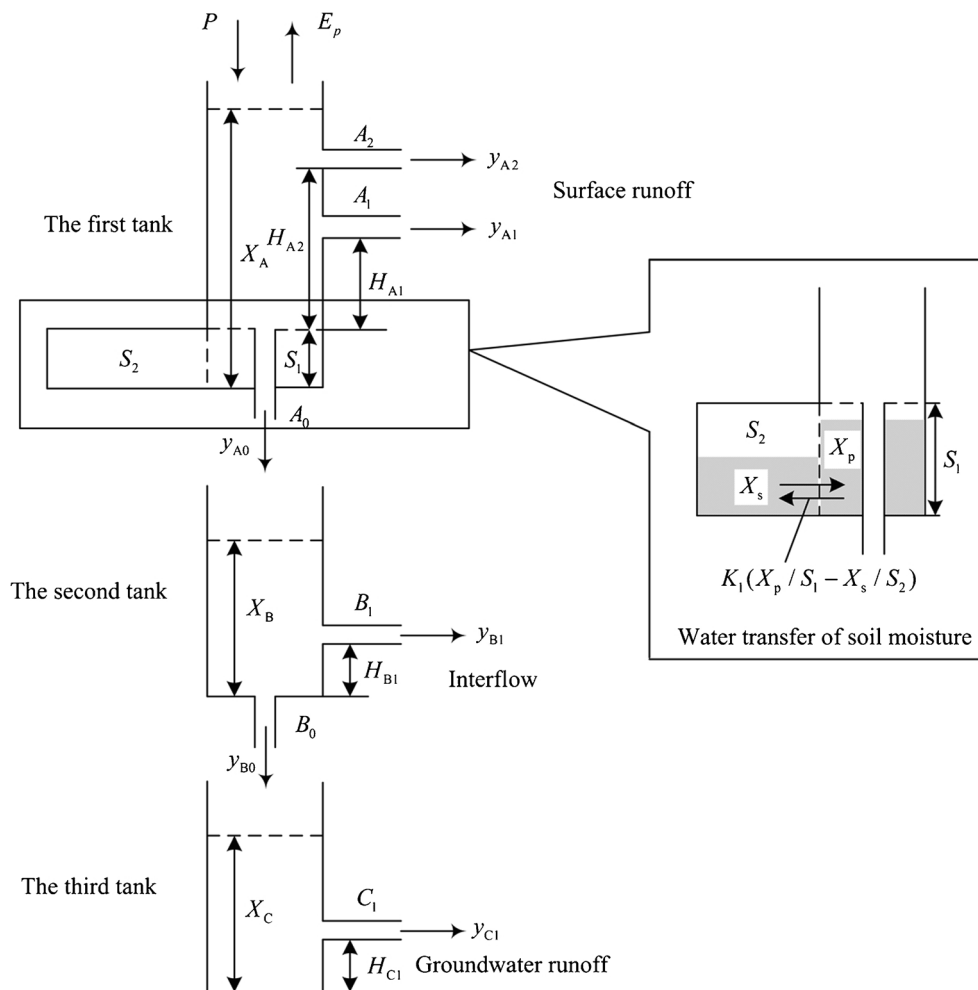
Study area

The study area is Hamajing catchment located in the west of Hubei Province, China at 29° 54'–30° 10' N latitude and 110°

10'–110° 35' E longitude (Fig. 4). The study catchment covers an area of 419 km² and includes two major rivers: Yuantougou river and Jiashaxi river. The average annual precipitation of the study site with a subtropical wet monsoon climate is 1171 mm, nearly 84.6% of which falls during the period from April to October. The elevation of the study area varies between 1300 and 2100 m above the sea level. Geological units include dolostone, thick and thin limestone, marlite, and Quaternary soil. As a typical karst catchment, Hamajing catchment has a lot of closed depressions. And most of these depressions are filled with deposited fine sediments from eroded top-soil and have been transformed into farmland (Meng et al. 2015). When floods occur, depressions will become storage places for water and reduce the total surface runoff (Fig. 5).

Because of the rural location, very limited observed data exist in the Hamajing catchment. The meteorological data including precipitation and evaporation at the Hamajing catchment are collected at daily scale from Jan 1, 2005 to Sep 30, 2005. The hydrological data comprise the daily river flow at the outlet of the

Fig. 1 Description of a grid in the hydrological model



Hamajing catchment. The river system of the Hamajing catchment is firstly obtained by a global digital elevation model (DEM) with a horizontal cell size of 30 m (<http://www.gscloud.cn>) and then adjusted according to the drainage map. By using the hydrology package of ARCGIS 10, the depression information in the whole catchment is obtained (Fig. 6). Using the centroids of depressions to judge the distance to the outlet of subcatchment, the runoff loss produced by karst depressions can be quantitatively assessed based on Eq. (1).

Results

Model calibration and verification

For a hydrological model, model calibration and verification are necessary procedures and essential before its application. Calibration consists in identifying the parameters of the model giving the minimum error between simulated and observed runoff data at the outlet of Hamajing catchment. To measure how good the agreement between the simulated and observed

Fig. 2 Flowchart of the hydrological model

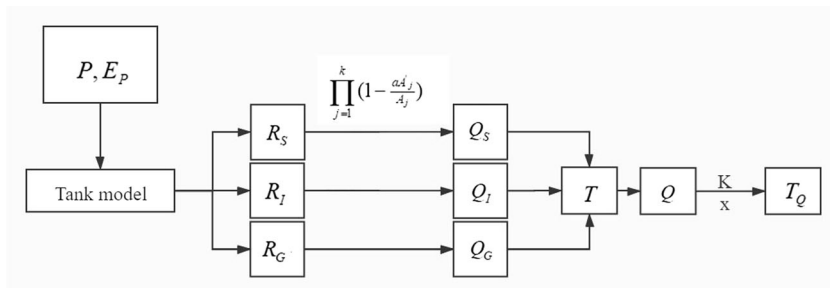
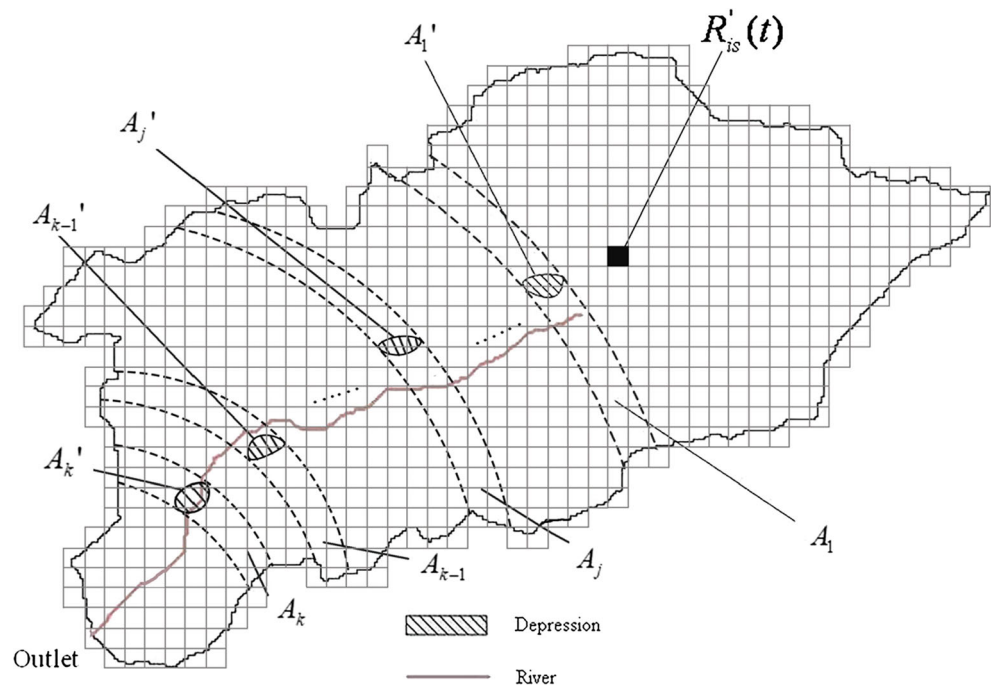


Fig. 3 Description of $R'_{is}(t)$, A'_j , and A_j in a subcatchment



runoff data is, model performance indicators need to be chosen. In our study, through reviewing literature, the following well-known two indicators are used (Meng et al., 2015; Oo et al., 2019):

Nash-Sutcliffe efficiency (NSE) : NSE

$$= 1 - \frac{\sum_{i=1}^n (C_i - O_i)^2}{\sum_{i=1}^n (O_i - \bar{O})^2} \tag{8}$$

where C_i is simulated runoff, O_i is observed runoff, \bar{O}_i is mean observed runoff, and n is the number of data samples. The closer NSE is to 1, the better the simulation result:

Root mean squared error (RMSE) : RMSE

$$= \sqrt{\frac{1}{n} \sum_{i=1}^n (C_i - O_i)^2} \tag{9}$$

The closer RMSE is to 0, the better the simulation result.

The aim of our study is to establish a conceptual hydrological model for simulating rainfall–runoff process in the karst region considering the role of karst depressions, as the small area and the strong consistency of soil and land use in this region, the runoff generation parameters of each grid are considered to be the same. Parameter calibration is firstly performed using the manual trial-and-error method. Then, the parameters used in the proposed conceptual hydrological model are optimized by a genetic algorithm which is a widely and effectively used method of parameter optimization in

hydrological model (Liong et al. 1995; Mohan 1997; Cheng et al. 2005; Wu and Chau 2006; Sidle et al. 2011). The initial values of parameters are given from the knowledge of catchment characteristics by some published studies (Nakagiri et al. 1998; Alam et al. 2006). The initial conditions used in the model are given from experience, and the starting period from Jan 1, 2005 to May 12, 2005 is used to eliminate the impact of initial conditions on the simulation results. During the calibration process, the simulations are run with the data from May 13, 2005 to Jul 13, 2005. The following time period from Jul 14, 2005 to Sep 30, 2005 is used to verify the identified parameter values. The results of calibrated parameters are shown in Table 2.

In addition, the proposed concept hydrological model requires many parameters. In order to improve the efficiency of parameter calibration and determine how these parameters affect simulation results, sensitivity analysis is carried out by using one factor at a time (OAT) screening technique to examine the relative sensitivity of NSE and RMSE to these parameters. In the OAT method, one factor, x_i , varies at a time, whereas other factors are fixed. A relative sensitivity index Z_i , the ratio between the relative normalized change in output to the normalized change in the related input, is calculated to quantify the sensitivity:

$$Z_i = \frac{dY}{dx_i} \frac{x_i}{Y} \tag{10}$$

where Z_i is sensitivity index with respect to parameter i indicating the relative partial effect of parameter x_i on modeled result Y .

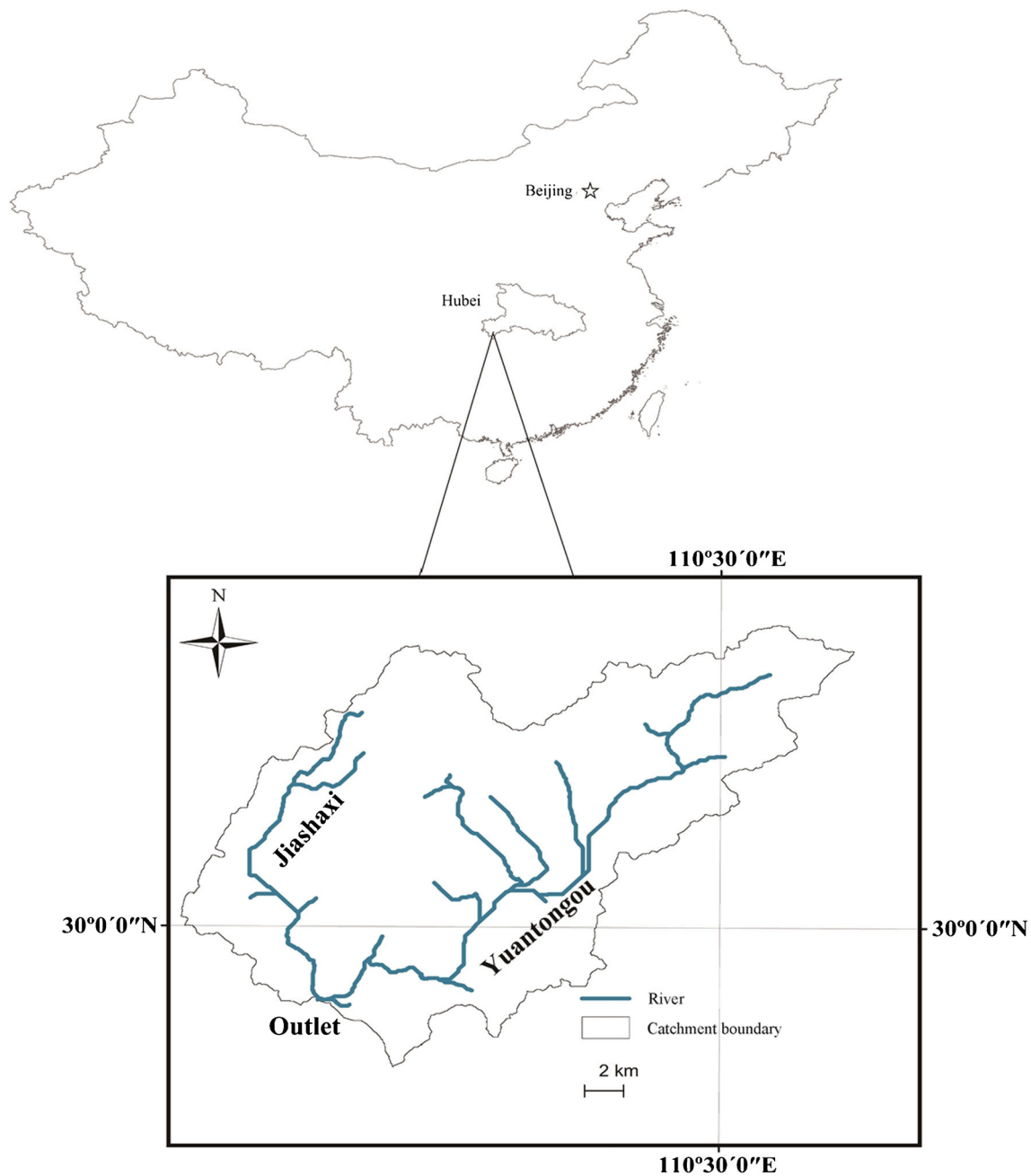


Fig. 4 Location map of the Hamajing catchment

Simulation results

Figure 7 depicts the simulation results at Hamajing catchment outlet considering the role of karst depressions. This simulation has a NSE of 0.85, RMSE of $6.24 \text{ m}^3/\text{s}$ during calibration period and NSE of 0.78, RMSE of $5.35 \text{ m}^3/\text{s}$ during validation period. Perrin et al. (2001) used 19 daily lumped hydrological models for runoff simulation within 429 catchments and illustrated that the mean NSE ranged from 0.39 to 0.51, while Su et al. (2001) applied the distributed Xin'anjiang model for runoff simulation in 9 catchments and reported

NSE values in the range 0.3–0.8 (mean value of approximately 0.65). Compared with these previously published values, the NSE values obtained in the proposed model are acceptable. The overall shape of the simulated runoff hydrograph generally shows good performance.

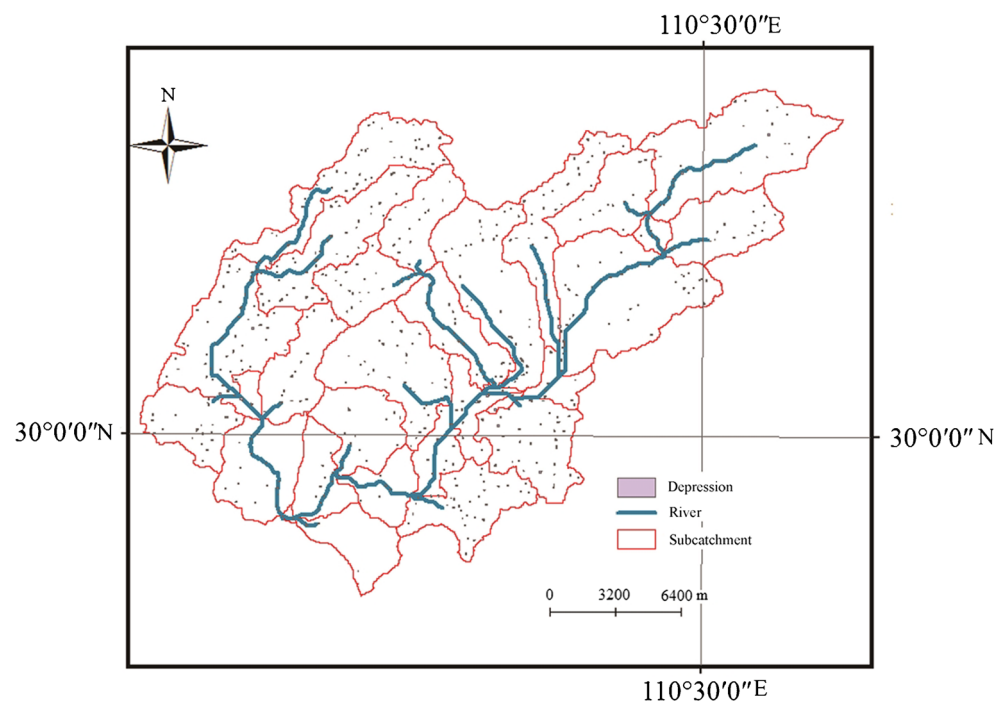
In order to analyze the influence of karst depressions on the simulation results, a scatter plot of simulated and observed daily runoff omitting karst depressions is displayed in Fig. 8. It could be seen that the correlation between the observed and simulated daily runoff is generally good with R^2 of about 0.83 and majority of points are above the 1:1 line indicating



Fig. 5 An inundated karst depression after a storm

remarkable over-prediction of daily runoff. The reason for this over-prediction is neglecting the water stored in karst depressions unable to be routed to the catchment outlet. From the 1:1 line shown in Fig. 9, the phenomenon of over prediction of the observed data is effectively avoided, and R^2 is improved from 0.83 to 0.86. Through introducing karst depression module, the proposed model is improved to be able to simulate runoff loss produced by karst depressions. and the calculated runoff is close to the actual value. For instance, a heavy rainfall event occurred on Jul 15, 2005, with a total rainfall of 128.8 mm, caused a peak flow of $71 \text{ m}^3/\text{s}$ at the outlet. The simulated peak flow by the model considering karst depressions is $79 \text{ m}^3/\text{s}$ compared with $106 \text{ m}^3/\text{s}$ regardless of karst depressions, about 50% greater than the observed value.

Fig. 6 Distribution of depressions extracted by DEM in Hamajing catchment



To get an all-around evaluation for performance of the proposed model in this study, comparison with previous model has been conducted. Meng et al. (2015) have developed a black box model based on artificial neural network model to simulate the runoff process in Hamajing catchment. The idea of threshold was used to divide the flow observations into flood period and non-flood period, which improved R^2 from 0.75 (ANN without threshold) to 0.83 (ANN with threshold, called T-ANN). Similar simulation results ($R^2 = 0.72\sim 0.87$) were recently obtained by applying the Emotion Neural Network model in simulating the rainfall–runoff process in an irrigation catchment, India (Kumar et al., 2019). It is noteworthy that the ANN-based black box models are meaningless of physical process. In contrast, the rainfall–runoff model proposed in this study is obviously advanced in considering the physical meaning of model structure.

Sensitivity analysis

A sensitivity analysis is conducted to determine the NSE and RMSE to variations in the parameters, which is beneficial for the calibration of the proposed model. Each parameter is adjusted independently to determine the change for the calibration period and varied by -20% , -10% , 10% , and 20% of the original value. Table 3 shows that the parameters related to the first tank are most sensitive to the simulation results, whereas the change of parameters related to the second and third tanks cannot significantly influence the simulation results. Additionally, the area ratio between karst depression and depression extracted by DEM in the catchment has great

Table 2 The results of calibrated parameters

y_{A0}	y_{A2}	y_{A1}	H_{A2} (mm)	H_{A1} (mm)	H_{B1} (mm)	y_{B1}	y_{B0}	H_{C1} (mm)	K_1 (mm)	y_c	S_1 (mm)	S_2 (mm)	α
0.22	0.25	0.13	31	9	5	0.11	0.1	5	12	0.05	70	185	0.41

influence on the simulation results, indicating the great impact of depression on the runoff process in karst catchment. Thus, adding this module is very important to simulate runoff loss produced by karst depressions, and it will also improve the simulation’s accuracy through reproducing the real hydrological processes in karst region.

Discussion

Bonacci (2001) described a phenomenon namely the limited discharge capacity of karst springs under high-water conditions caused by intense precipitation. The limitation on the maximum flow rate of the karst catchment is ascribed to six reasons: limited size of the karst conduit, flow under pressure, intercatchment overflow, overflow from a main spring to intermittent springs, available water storage in karst depressions, and other factors such as climate, soil and vegetation cover, and altitude and geological conditions. In this paper, a conceptual hydrological model considering runoff loss produced by karst depressions, one of these factors mentioned above, is established to simulate the hydrological processes of karst catchment.

Although the daily values of runoff simulation match closely with their observed data by adding karst depression module, some of the peak flows especially middle and small floods are under predicted. For example, a moderate rainfall event occurred on Aug 29, 2005, with a total rainfall of 46 mm, caused a peak flow of 41 m³/s at the outlet, while the

simulated peak flow by the model including karst depression module was only 27 m³/s, 34% less than the observed value. Therefore, there is still room for the improvement of the proposed model. In addition, the proposed model cannot reproduce the natural flow variability during non-flood periods. It may be ascribed to the small area of the study catchment, leading to nearly zero flow in non-flood periods. And this low flow is significantly affected by random disturbance (Meng et al. 2015). Future study may give more attention to the influence of karst depressions on different degrees of peak floods, and it is necessary to get a better understanding of the physical processes for water stored in karst depressions. Perhaps a more detailed description of the karst catchment area and catchment soil properties can also improve the model performance.

Summary and conclusions

In this study, a conceptual hydrological model for karst catchments is proposed and tested to simulate runoff processes impacted by karst depressions, which is important and rarely reported. In the runoff generation process, a three-serial tank model coupled with two soil tanks is used to simulate the surface runoff, interflow, groundwater runoff, and soil moisture. During the process of flow concentration, surface runoff from each grid is reduced by karst depressions at its lower reach, and this runoff loss is calculated based on the area ratio of karst depression. River channel routing is carried out

Fig. 7 The simulation results considering karst depressions at Hamajing catchment outlet

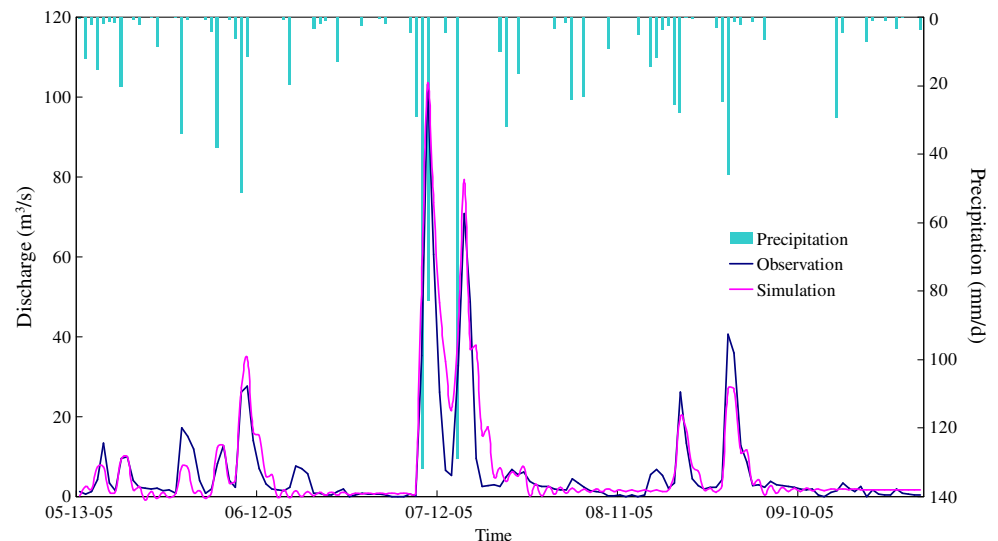
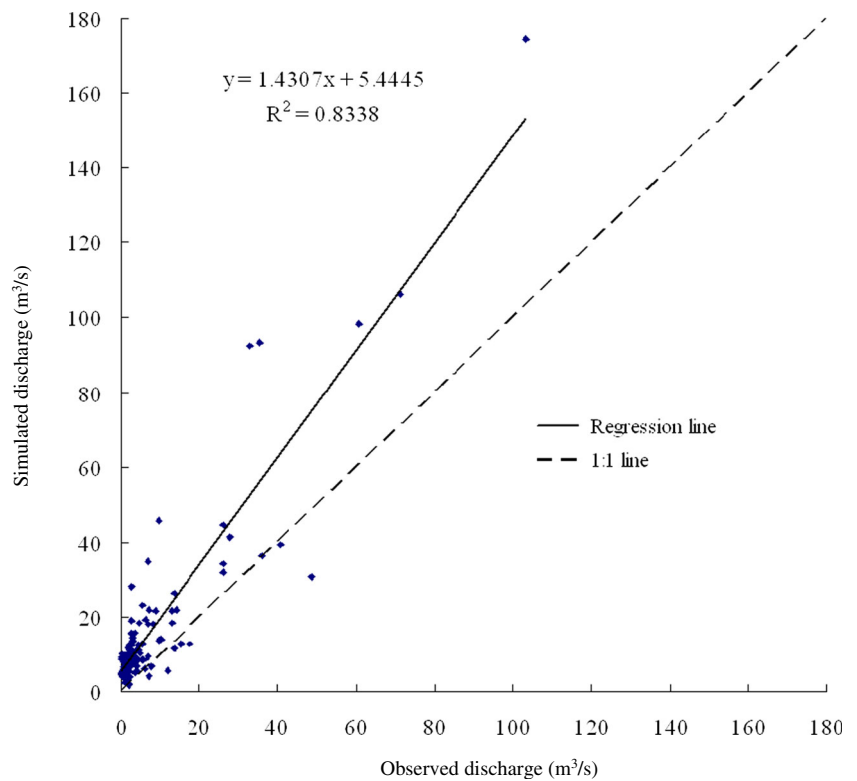


Fig. 8 Comparison between the observed and simulated daily discharge (without considering karst depressions)



through Muskingum model. This proposed model is applied to a small karst catchment—Hamajing catchment—located in the west of Hubei Province, China. The satisfactory performance of the proposed model further confirms the importance of considering the impact of karst depression in simulating

rainfall–runoff processes in karst catchment. Sensitivity analysis reveals that the parameters related to the first tank are most sensitive to the simulation results, and the area ratio of karst depression has great influence on the simulation of runoff processes in karst catchment.

Fig. 9 Comparison between the observed and simulated daily discharge (considering karst depressions)

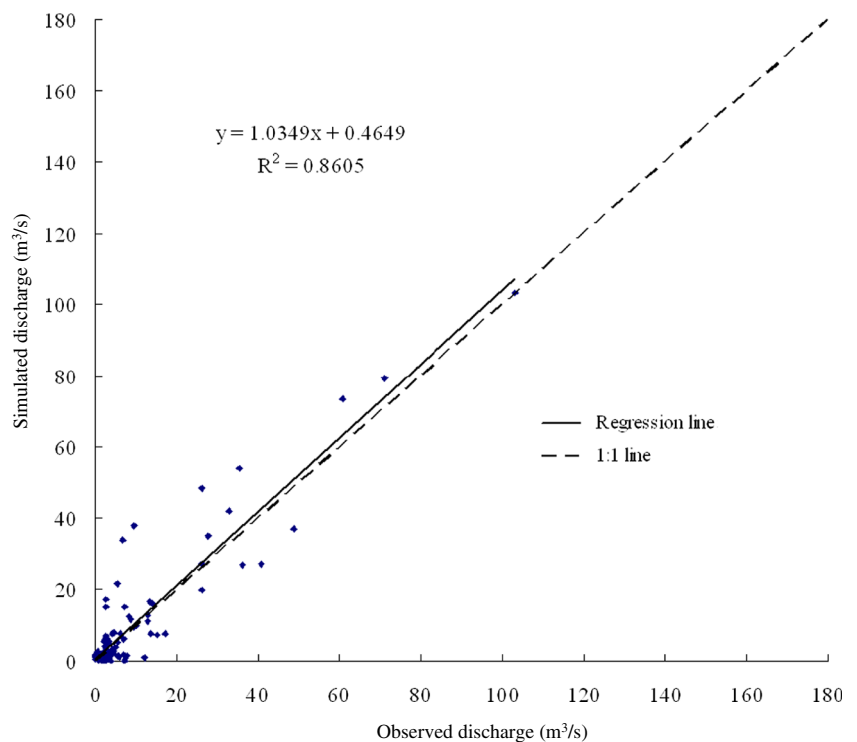


Table 3 Sensitivities of parameters for the case of hydrological model

	NSE				RMSE			
	10%	- 10%	20%	- 20%	10%	- 10%	20%	- 20%
y_{A0}	0.627	0.882	0.523	1.078	- 0.287	- 0.390	- 0.242	- 0.465
y_{A2}	- 1.000	- 0.942	- 1.030	- 0.910	0.443	0.434	0.445	0.429
y_{A1}	- 1.982	- 1.723	- 2.108	- 1.578	0.858	0.810	0.875	0.771
H_{A2}	1.246	1.319	1.217	1.409	- 0.579	- 0.578	- 0.583	- 0.600
H_{A1}	0.110	0.127	0.100	0.136	- 0.050	- 0.057	- 0.045	- 0.061
H_{B1}	1.06E-04	1.09 E-04	1.04 E-04	1.11 E-04	- 4.8E-05	- 4.9E-05	- 4.7E-05	- 5E-05
y_{B1}	- 0.018	- 0.018	- 0.018	- 0.017	8.11 E-03	7.92 E-03	8.28 E-03	7.58 E-03
y_{B0}	3.27E-04	2.83E-04	3.36E-04	2.59E-04	- 1.47E-04	- 1.28E-04	- 1.51E-04	- 1.17E-04
H_{C1}	6.70E-04	5.86E-04	7.04E-04	5.70E-04	- 3.02E-04	- 2.64E-04	- 3.18E-04	- 2.57E-04
y_{C1}	- 3.41 E-03	- 3.41 E-03	- 3.41 E-03	- 3.41 E-03	1.54 E-03	1.54 E-03	1.54 E-03	1.54 E-03
K_1	- 0.036	- 0.021	- 0.018	- 0.026	0.081	0.046	0.041	0.058
S_1	0.072	0.039	0.036	0.052	- 0.033	- 0.018	- 0.016	- 0.023
S_2	6.29 E-03	7.58 E-03	5.80 E-03	8.44 E-03	- 2.84 E-03	- 3.42 E-03	- 2.62 E-03	- 3.81 E-03
α	1.006	1.121	0.992	1.177	- 0.302	- 0.371	- 0.272	- 0.396

Compared with existing rainfall–runoff model, the proposed model belongs to conceptual hydrological model with the characteristics of simple structure and computational efficiency. Only the precipitation, pan evaporation, and the DEM data are required to run this model, which is suitable for simulating hydrological processes in karst catchment with limited observed data. Conclusively, the proposed model could, therefore, be a successful alternative conceptual hydrological model for karst catchments because of its convenience, clear physical implications, and improved accuracy. However, more research work should be conducted in the future to verify the applicability and parameter estimation of the proposed model.

Funding This research was funded by the National Natural Science Foundation of China (51979252) and the Fundamental Research Funds for the Central Universities, China University of Geosciences (Wuhan) (CUGCJ1822).

References

- Alam AHMB, Takeuchi J, Kawachi T (2006) Development of distributed rainfall-runoff model incorporating soil moisture model. *Transac Japan Soc Irrig Drain Reclam Eng* 244:29–37
- Amin MGM, Veith TL, Collick AS, Karsten HD, Buda AR (2017) Simulating hydrological and nonpoint source pollution processes in a karst watershed: a variable source area hydrology model evaluation. *Agr Water Manag* 180:212–223. <https://doi.org/10.1016/j.agwat.2016.07.011>
- Barrett ME, Charbeneau RJ (1997) A parsimonious model for simulating flow in a karst aquifer. *J Hydrol* 196(1-4):47–65. [https://doi.org/10.1016/S0022-1694\(96\)03339-2](https://doi.org/10.1016/S0022-1694(96)03339-2)
- Bonacci O (2001) Analysis of the maximum discharge of karst springs. *Hydrogeol J* 9(4):328–338. <https://doi.org/10.1007/s100400100142>
- Campbell CW, Sullivan SM (2002) Simulating time-varying cave flow and water levels using the Storm Water Management Model. *Eng Geol* 65(2-3):133–139. [https://doi.org/10.1016/S0013-7952\(01\)00120-X](https://doi.org/10.1016/S0013-7952(01)00120-X)
- Cheng CT, Wu XY, Chau KW (2005) Multiple criteria rainfall-runoff model calibration using a parallel genetic algorithm in a cluster of computer. *Hydrol Sci J* 50(6):1069–1087. <https://doi.org/10.1623/hysj.2005.50.6.1069>
- Dreiss SJ (1982) Linear kernels for karst aquifers. *Water Resour Res* 18(4):865–876. <https://doi.org/10.1029/WR018i004p00865>
- Dreiss SJ (1983) Linear unit-response functions as indicators of recharge areas for large karst springs. *J Hydrol* 61(1-3):31–44. [https://doi.org/10.1016/0022-1694\(83\)90233-0](https://doi.org/10.1016/0022-1694(83)90233-0)
- Eisenlohr L, Kiral L, Bouzelboudjen M, Rossier Y (1997) Numerical simulation as a tool for checking the interpretation of karst spring hydrographs. *J Hydrol* 193(1-4):306–315. [https://doi.org/10.1016/S0022-1694\(96\)03140-X](https://doi.org/10.1016/S0022-1694(96)03140-X)
- Fan YH, Huo XL, Hao YH, Liu Y, Wang TK, Liu YC, Yeh TCJ (2013) An assembled extreme value statistical model of karst spring discharge. *J Hydrol* 504:57–68. <https://doi.org/10.1016/j.jhydrol.2013.09.023>
- Felton GK, Currens JC (1994) Peak flow rate and recession-curve characteristics of a karst spring in the Inner Bluegrass, central Kentucky. *J Hydrol* 162(1-2):119–141. [https://doi.org/10.1016/0022-1694\(94\)90006-X](https://doi.org/10.1016/0022-1694(94)90006-X)
- Freeze RA, Harlan RL (1969) Blueprint for a physically-based, digitally-simulated hydrologic response model. *J Hydrol* 9(3):237–258. [https://doi.org/10.1016/0022-1694\(69\)90020-1](https://doi.org/10.1016/0022-1694(69)90020-1)
- Halihan T, Wicks CM (1998) Modeling of storm responses in conduit flow aquifers with reservoirs. *J Hydrol* 208(1-2):82–91. [https://doi.org/10.1016/S0022-1694\(98\)00149-8](https://doi.org/10.1016/S0022-1694(98)00149-8)
- Hao YH, Yeh TC, Gao ZQ, Wang YR, Zhang Y (2006) A gray system model for studying the responses to climatic change: the Liulin karst springs, China. *J Hydrol* 328(3-4):668–676. <https://doi.org/10.1016/j.jhydrol.2006.01.022>
- Hu HP, Tian FQ (2007) Advancement in research of physically based watershed hydrological model. *J Hydraul Eng* 38(5):511–517 (in Chinese)

- Hu CH, Hao YH, Yeh TC, Pang B, Wu ZN (2008) Simulation of spring flows from a karst aquifer with an artificial neural network. *Hydrol Process* 22(5):596–604. <https://doi.org/10.1002/hyp.6625>
- Huang W, Nakane K, Matsuura R, Matsuura T (2007) Distributed tank model and GAME reanalysis data applied to the simulation of runoff within the Chao Phraya River Basin, Thailand. *Hydrol Process* 21(15):2049–2060. <https://doi.org/10.1002/hyp.6710>
- Jukic D, Denic-Jukic V (2006) Nonlinear kernel functions for karst aquifers. *J Hydrol* 328(1–2):360–374. <https://doi.org/10.1016/j.jhydrol.2005.12.030>
- Kumar S, Roshni T, Himayoun D (2019) A comparison of emotional neural network (ENN) and artificial neural network (ANN) approach for rainfall-runoff modelling. *Civil Eng J* 5(10):2120–2130. <https://doi.org/10.28991/cej-2019-03091398>
- Labat D, Ababou R, Mangin A (2000a) Rainfall-runoff relations for karstic springs. Part I: convolution and spectral analyses. *J Hydrol* 238(3–4):123–148. [https://doi.org/10.1016/S0022-1694\(00\)00321-8](https://doi.org/10.1016/S0022-1694(00)00321-8)
- Labat D, Ababou R, Mangin A (2000b) Rainfall-runoff relations for karstic springs. Part II: continuous wavelet and discrete orthogonal multiresolution analyses. *J Hydrol* 238(3–4):149–178. [https://doi.org/10.1016/S0022-1694\(00\)00322-X](https://doi.org/10.1016/S0022-1694(00)00322-X)
- Labat D, Ababou R, Mangin A (2001) Introduction of wavelet analyses to rainfall/runoffs relationship for a karstic basin: the case of Licq-Atherey karstic system (France). *Ground Water* 39(4):605–615. <https://doi.org/10.1111/j.1745-6584.2001.tb02348>
- Lambrakis N, Andreou AS, Polydoropoulos P, Georgopoulos E, Bountis T (2000) Nonlinear analysis and forecasting of a brackish karstic spring. *Water Resour Res* 36(4):875–884. <https://doi.org/10.1029/1999WR900353>
- Li YB, Shao JA, Wang SJ, Wei ZF (2006) A conceptual analysis of karst ecosystem fragility. *Proc Geogr* 25(5):1–9 (in Chinese). <https://doi.org/10.11820/dlkxjz.2006.05.001>
- Li J, Yuan DX, Liu J, Jiang YJ, Chen YB, Hsu KL, Sorooshian S (2019) Predicting floods in a large karst river basin by coupling PERSIANN-CCS QPEs with a physically based distributed hydrological model. *Hydrol Earth Syst Sci* 23(3):1505–1532. <https://doi.org/10.5194/hess-23-1505-2019>
- Liong SY, Chan WT, ShreeRam J (1995) Peak-flow forecast with genetic algorithm and SWMM. *J Hydraul Eng* 121(8):613–617. [https://doi.org/10.1061/\(ASCE\)0733-9429\(1995\)121:8\(613\)](https://doi.org/10.1061/(ASCE)0733-9429(1995)121:8(613))
- Liu YB, Batelaan O, De Smedt F, Huong NT, Tam VT (2005) Test of a distributed modelling approach to predict flood flows in the karst Suoimuoi catchment in Vietnam. *Environ Geol* 48(7):931–940. <https://doi.org/10.1007/s00254-005-0031-1>
- Mangin A (1975) Contribution à l'étude hydrodynamique des aquifères karstiques. *Ann Spéléologie* 29:283–332
- McCarthy GT (1938) The unit hydrograph and flood routing. Conf. North Atlantic Division, U.S. Army Corps of Engineers., U.S. Engrs., Ofc., Providence, R.I.
- Meng XM, Yin MS, Ning LB, Liu DF, Xue XW (2015) A threshold artificial neural network model for improving runoff prediction in a karst watershed. *Environ Earth Sci* 74(6):5039–5048. <https://doi.org/10.1007/s12665-015-4562-9>
- Mohan S (1997) Parameter estimation of nonlinear Muskingum models using genetic algorithm. *J Hydraul Eng* 123(2):137–142. [https://doi.org/10.1061/\(ASCE\)0733-9429\(1997\)123:2\(137\)](https://doi.org/10.1061/(ASCE)0733-9429(1997)123:2(137))
- Nakagiri T, Watanabe T, Horino H, Maruyama T (1998) Development of a hydrological system model in the Kino River Basin—analysis of irrigation water use by a hydrological system model (I). *Transac Japan Soc Irrig Drain Reclam Eng* 198:1–11
- Oo HT, Zin WW, Kyi CCT (2019) Assessment of future climate change projections using multiple global climate models. *Civil Eng J* 5(10):2152–2166. <https://doi.org/10.28991/cej-2019-03091401>
- Padilla A, Pulido-Bosch A (2008) Simple procedure to simulate karstic aquifers. *Hydrol Process* 22(12):1876–1884. <https://doi.org/10.1002/hyp.6772>
- Palanisamy B, Workman SR (2015) Hydrologic modeling of flow through sinkholes located in streambeds of Cane Run Stream, Kentucky. *J Hydrol Eng* 20(5):04014066. [https://doi.org/10.1061/\(ASCE\)HE.1943-5584.0001060](https://doi.org/10.1061/(ASCE)HE.1943-5584.0001060)
- Perrin C, Michel C, Andreassian V (2001) Does a large number of parameters enhance model performance? Comparative assessment of common catchment model structures on 429 catchments. *J Hydrol* 242(3–4):275–301. [https://doi.org/10.1016/S0022-1694\(00\)00393-0](https://doi.org/10.1016/S0022-1694(00)00393-0)
- Sidle RC, Kim K, Tsuboyama Y, Hosoda I (2011) Development and application of a simple hydrogeomorphic model for headwater catchments. *Water Resour Res* 47:W00H13. <https://doi.org/10.1029/2011WR010662>
- Su B, Lu M, Kazama S, Sawamoto M (2001) Runoff simulation and its impact on water quality in the Kamafusa lake catchment. Proceedings of XXIX IAHR Congress, Beijing, China; Theme A: 292–299
- Sugawara M (1972) *River Discharge Analyses*. Kyoritsu Press, Tokyo, pp 1–257 (in Japanese)
- Sun AY, Painter SL, Green RT (2005) Modeling Barton Springs segment of the Edwards aquifer using MODFLOW-DCM. Proceedings of Sinkholes and the Engineering and Environmental Impacts of Karst. 163–177
- WMO (World Meteorological Organization) (1981) Tank model, HOMS Component J04•1•01. <http://www.wmo.ch/web/homs/projects/homs/j04101.html> ()
- Wu CL, Chau KW (2006) A flood forecasting neural network model with genetic algorithm. *Int J Environ Pollut* 28(3–4):261–273. <https://doi.org/10.1504/IJEP.2006.011211>
- Zhang ZC, Chen X, Ghadouani A, Shi P (2011) Modelling hydrological processes influenced by soil, rock and vegetation in a small karst basin of southwest China. *Hydrol Process* 25(15):2456–2470. <https://doi.org/10.1002/hyp.8022>